Chemical Science

ROYAL SOCIETY OF CHEMISTRY

EDGE ARTICLE

View Article Online
View Journal | View Issue

Cite this: *Chem. Sci.*, 2025, **16**, 10340

All publication charges for this article have been paid for by the Royal Society of Chemistry

A thermally and photoresponsive luminescent single-molecule magnet based on dysprosium–anthracene: effect of temperature on anthracene photocycloaddition†

Xiu-Fang Ma, ‡[a] Xin-Lan Hou,‡[b] Ye-Hui Qin,[a] Qian Teng,[a] Song-Song Bao,[a] Yu-Xi Tian *[b] and Li-Min Zheng *[a]

Received 19th February 2025
Accepted 17th April 2025

DOI: 10.1039/d5sc01302j

rsc.li/chemical-science

Stimuli-responsive lanthanide-based single-molecule magnets (Ln-SMMs) are attractive for their potential in information storage, sensors and molecular devices. However, challenges remain in synergistically tuning the magnetic and optical properties of Ln-SMMs at the same temperature. Herein, we report a mononuclear dysprosium complex containing anthracene units, namely $[Dy(SeCN)_2(NO_3)(depma)_2(4\text{-hpy})_2]$ (**1DySeCN**) (depma = 9-diethylphosphonomethylanthracene, 4-hpy = 4-hydroxypyridine). It shows a thermally induced phase transition attributed to an order–disorder transition of the axial 4-hpy ligand, and a thermochromism due to a slight slipping of the anthracene pairs. Compound **1DySeCN** can undergo [4 + 4] photocycloaddition reaction in a single-crystal-to-single-crystal (SC–SC) transformation manner at room temperature to form the 1D coordination polymer $[Dy(SeCN)_2(NO_3)(depma_2)(4\text{-hpy})_2]_n$ (**2DySeCN**), accompanied by a luminescence switch from yellow to blue-white. Meanwhile, significant changes in SMM properties are observed with the reduction of energy barrier from 334 K to 144 K and the narrowing of the butterfly-like hysteresis loop. We further investigated the effect of temperature on the photodimerization reaction of anthracene in **1DySeCN**, and found that the compound can still undergo efficient photodimerization at temperatures as low as 200 K. At this temperature, the magnetic susceptibility ($\chi_M T$) value of the dilute compound **1DySeCN@Y** also changed significantly before and after light irradiation. This study provides the first example of lanthanide–anthracene compounds synergistically modulating the magnetic and luminescent properties at the same temperature.

Introduction

Molecular materials showing light-responsive magnetic and luminescent properties have received considerable attention in recent years owing to their potential applications in molecular spintronics, sensors, and devices.[1–4] Lanthanide-based single-molecule magnets (Ln-SMMs) are appealing because they not only exhibit characteristic photoluminescence (PL) associated with the f–f/d–f electronic transitions, but also the strong magnetic anisotropy arising from spin–orbit coupling.[5–11] However, although the magnetic properties of Ln-SMMs are sensitive to external stimuli,[12–15] their luminescent properties are not easily modulated. So far, reports on the synergistic modulation of the magnetic and luminescent properties of Ln-SMMs are still rare,[16] which have been realized by external stimuli such as solvent exchange or removal,[17,18] mechanical force,[19] and light irradiation.[20–26] The latter is particularly desired because light can be manipulated quickly and easily. Recent work has shown that the incorporation of photoactive components into Ln-SMMs can achieve changes in SMM and optical properties such as photochromism[20–22] and photoswitchable luminescence.[23–26] For example, Wang and coworkers found that photogenerated radicals from organic guest molecules induced a switch in the SMM behavior of a Dy chain compound as well as a decrease in luminescence intensity.[23] We found that lanthanide–anthracene compounds can undergo reversible [4 + 4] photocycloaddition reaction, accompanied by dramatic changes in magnetic and luminescent

[a]*State Key Laboratory of Coordination Chemistry, School of Chemistry and Chemical Engineering, Collaborative Innovation Center of Advanced Microstructures, Nanjing University, Nanjing 210023, China. E-mail: lmzheng@nju.edu.cn*

[b]*State Key Laboratory of Analytical Chemistry for Life Science, Key Laboratory of Mesoscopic Chemistry of MOE, School of Chemistry and Chemical Engineering, Nanjing University, Nanjing 210023, China. E-mail: tyx@nju.edu.cn*

† Electronic supplementary information (ESI) available: Experimental details, crystallographic details, and full characterization (SC-XRD, PXRD, IR, UV-vis and photoluminescence spectra, thermal analysis, photographs) of all described compounds. CCDC 2421525–2421527, 2424230 and 2424231. For ESI and crystallographic data in CIF or other electronic format see DOI: https://doi.org/10.1039/d5sc01302j

‡ These authors contributed equally to this work.

properties.[26–31] Notably, the temperature at which the photocycloaddition occurred for Dy–anthracene complexes did not generally coincide with the temperature at which the magnetic changes were observed, the former usually at room temperature and the latter at very low temperatures. This raises the question about what is the minimum temperature at which the photocycloaddition reaction of lanthanide–anthracene complexes can efficiently take place? Can the modulation of their magnetic and luminescent properties be achieved by photo-stimulation at the same temperature?

To address these questions, we herein report a new Dy–anthracene complex, $[Dy(SeCN)_2(NO_3)(depma)_2(4\text{-hpy})_2]$ (**1DySeCN**, 4-hpy = 4-hydroxypyridine, depma = 9-diethylphosphonomethylanthracene, Scheme 1), and its photophysical, photochemical and magnetic properties at and below room temperature. **1DySeCN** was designed and synthesized because of its structural similarity to the previously reported compound $[Dy(SCN)_2(NO_3)(depma)_2(4\text{-hpy})_2]$ (**DySCN**, Scheme 1)[31] except for the replacement of SCN^- with $SeCN^-$. We envisioned that the incorporation of $SeCN^-$ would lead to a weakening of the Dy–N bond at the equatorial position, which in turn would enhance the magnetic anisotropy. Indeed, **1DySeCN** shows SMM behaviour at zero dc field with an effective energy barrier (U_{eff}) of 334 K, which is higher than that of **DySCN** (U_{eff} = 277 K). The dilute sample **1DySeCN@Y** displays an open butterfly-shaped magnetic hysteresis below the blocking temperature (T_B = 4.2 K) with a coercivity (H_c) of 1200 Oe at 2.0 K. To the best of our knowledge, the U_{eff}, T_B and H_c values are the highest among the known photoresponsive luminescent Ln-SMMs. In addition, **1DySeCN** undergoes photocycloaddition reaction in a single-crystal-to-single-crystal (SC–SC) manner at room temperature to form a 1D chain compound $[Dy(SeCN)_2(NO_3)(depma_2)(4\text{-hpy})_2]_n$ (**2DySeCN**, $depma_2$ is the photo-dimerized depma), accompanied by remarkable changes in photoluminescent (PL) and magnetic properties. Interestingly, the photocycloaddition reaction of **1DySeCN** can occur at temperatures down to 140 K. The *in situ* PL measurements on a single crystal of **1DySeCN** revealed a significant photo-induced change in luminescence when the temperature was as low as 200 K. Impressively, the dilute sample **1DySeCN@Y** showed photo-triggered luminescence and magnetic changes at 200 K. This work opens up the possibility of synergistically modulating the magnetic and luminescent properties of Ln-SMMs by photocycloaddition at the same temperature.

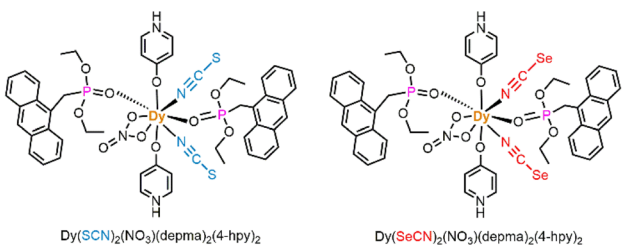

Scheme 1 Molecular structures of compounds **DySCN** (left) and **1DySeCN** (right).

Results and discussion

Crystal structure of 1DySeCN and its reversible thermally induced SC–SC structural transformation

Compound **1DySeCN** was obtained by the reaction of $Dy(NO_3)_3\cdot 6H_2O$, KSeCN, 4-hpy, and depma in CH_3CN (Scheme S1†). The purity was confirmed by the PXRD measurement (Fig. S1†). Single crystal structural analysis of **1DySeCN** at 293 K (named **1DySeCN-293**) reveals that it crystallizes in the monoclinic system, space group $P2_1/m$ (Tables 1 and S1†). The asymmetric unit contains 0.5 Dy^{III} ion, one $SeCN^-$, 0.5 NO_3^-, one depma and two half 4-hpy ligands. The Dy^{III} ion is eight-coordinated, surrounded by two N atoms from two $SeCN^-$, and six O atoms from one NO_3^-, two depma, and two 4-hpy ligands (Fig. 1a and Table S2†). The SHAPE 2.1 calculation suggests that the geometry of $\{DyN_2O_6\}$ is close to the Snub diphenoid J84 (D_{2d}) (CShM = 1.802) (Table S3†).[32] However, if we consider the chelating NO_3^- as occupying one coordination site, the geometry of Dy^{III} can be viewed as having a pseudo-D_{5h} symmetry with the two axial positions filled with O atoms from the zwitterionic 4-hpy ligands [Dy1–O_{ax}: 2.208(9), 2.231(8) Å; ∠O7–Dy1–O8: 163.2(4)°; Dy1–O/N_{eq}: 2.313(9)–2.576(8) Å]. The neighbouring molecules are stacked through face-to-face π–π interacting anthracene rings to form a one-dimensional (1D) supramolecular chain (Fig. 1b). The centre-to-centre (d_{cc}) and plane-to-plane (d_{pp}) distances of the two anthracene rings are 3.759 Å and 3.428 Å, respectively, which satisfy the Schmidt's rule for photocycloaddition reaction.[33] The chains are further connected by multiple hydrogen bonds of N–H···O/Se and C–H···O, thus providing a flexible supramolecular network that may tolerate structural changes induced by photocycloaddition reaction (Fig. S2 and Table S4†). In addition, we note that the axial Dy–O_{ax} bond lengths in **1DySeCN-293** (2.208/2.231 Å) are slightly shortened compared with those in **DySCN** (2.210/2.239 Å), while the Dy1–N_{eq} bond lengths (2.462 Å *vs.* 2.456 Å in **DySCN**) and the shortest Dy···Dy distance are slightly elongated (9.754 Å *vs.* 9.54 Å in **DySCN**),[31] suggesting that the magnetic anisotropy could be further enhanced in **1DySeCN**.

Since one of the two 4-hpy ligands in **1DySeCN** is disordered at 293 K, we measured the differential scanning calorimetry (DSC) curve to examine whether an order–disorder phase transition may occur. As shown in Fig. 2 and S3,† the DSC curve of **1DySeCN** shows an exothermic peak at 276 K upon cooling and an endothermic peak at 292 K upon warming (ΔT = 16 K). Based on the endothermic peak, we can calculate the enthalpy change (ΔH) to be 1.29 kJ mol^{-1}, and the entropy change (ΔS) to be 4.42 J mol^{-1} K^{-1}. According to the Boltzmann equation $\Delta S = R\ln(N)$, where R is the gas constant and N represents the number of disordered states, the value N was estimated to be 1.69, suggesting that the phase transition originates from the order–disorder transition of the axial 4-hpy ligand.[34] The thermo-induced phase transition of **1DySeCN** was also confirmed by variable temperature PXRD measurements (Fig. S4†). Notably, an order–disorder phase transition was not observed for the related compound **DySCN** down to 193 K, though one of the two axial 4-hpy ligands was also disordered in the latter.[31]

Table 1 Comparison of the cell and structural parameters in **1DySeCN** and **2DySeCN** measured at different temperatures

Complex	1DySeCN-293	1DySeCN-193	1DySeCN-130	2DySeCN-293	2DySeCN-193
Temperature	293 K	193 K	130 K	293 K	193 K
Crystal system	Monoclinic	Triclinic	Triclinic	Monoclinic	Monoclinic
Space group	$P2_1/m$	$P\bar{1}$	$P\bar{1}$	$P2_1/m$	$P2_1/m$
a (Å)	9.7539(12)	9.6729(5)	9.7055(12)	9.585(9)	9.5847(12)
b (Å)	25.787(3)	11.1667(6)	11.1138(13)	25.97(2)	25.809(3)
c (Å)	11.2182(14)	25.6156(16)	25.416(3)	11.340(12)	11.2751(13)
α (°)	90	90.315(2)	90.469(3)	90	90
β (°)	111.587(4)	92.411(2)	92.518(4)	112.620(19)	112.946(3)
γ (°)	90	112.001(2)	112.134(3)	90	90
V (Å^3)	2623.8(5)	2562.4(3)	2536.1(5)	2606(4)	2568.4(6)
Dy–O (axial)/Å	2.208/2.231	2.228/2.240	2.227/2.243	2.250/2.222	2.219/2.225
Dy–O (equatorial)/Å	2.313–2.576	2.317–2.563	2.310–2.557	2.307–2.568	2.326–2.546
Dy–N/Å	2.463	2.464/2.468	2.462/2.474	2.456	2.459
O–Dy–O (axial)/°	163.2	162.0	162.2	163.2	162.4
Dy⋯Dy/Å	9.754	9.673	9.705	9.584	9.585
Slip angle θ/°	21.91	22.04/23.03	22.44/24.49	—	—
d_{cc}/Å	3.759	3.835/3.713	3.846/3.685	—	—
d_{pp}/Å	3.428	3.433/3.439	3.418/3.442	—	—
d_{C2-C9A}/Å	3.753	3.832/3.707	3.843/3.664	1.658	1.645

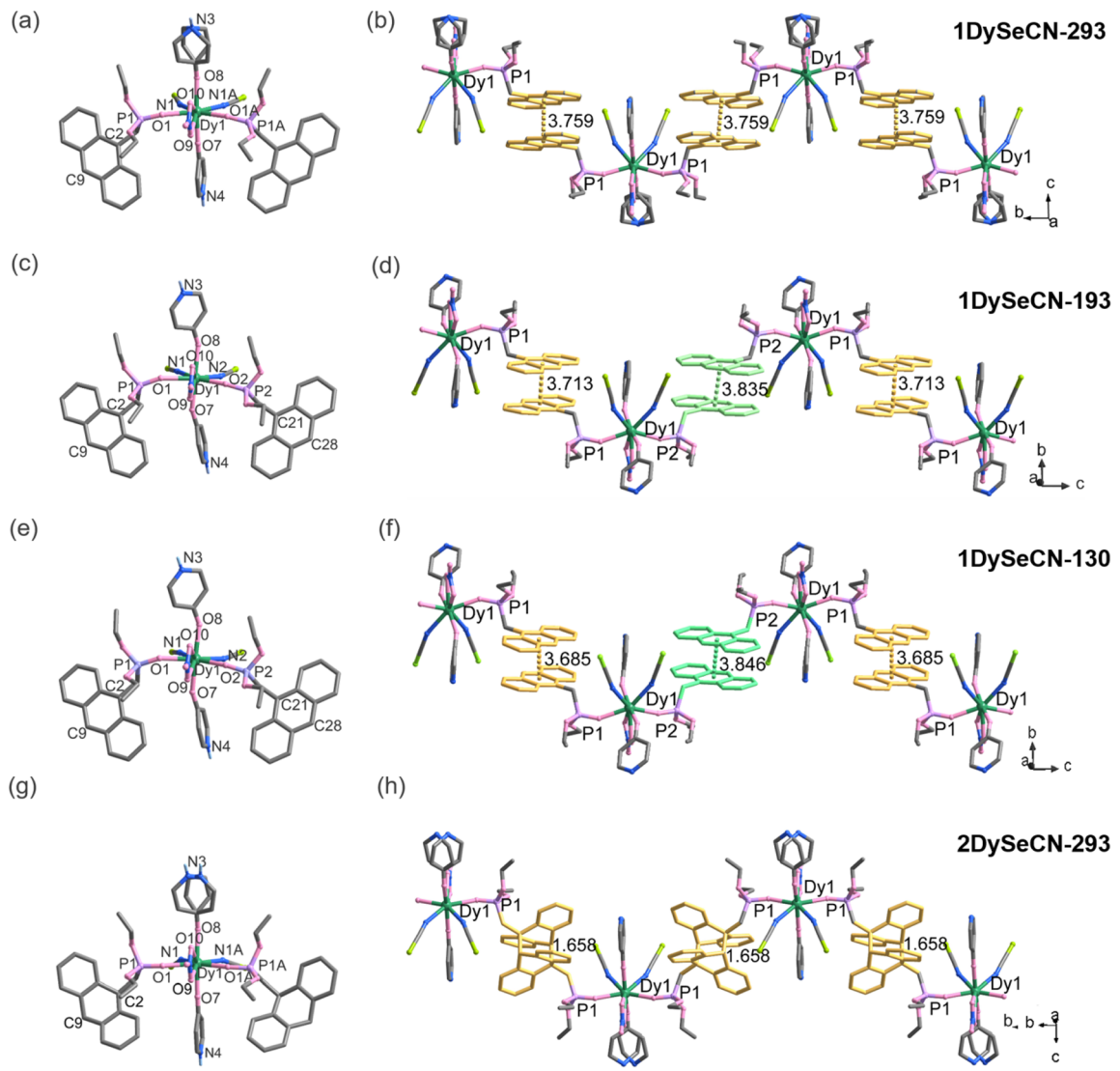

Fig. 1 The molecule structures (a, c, e and g) and 1D chain (b, d, f and h) of **1DySeCN-293**, **1DySeCN-193**, **1DySeCN-130** and **2DySeCN-293**.

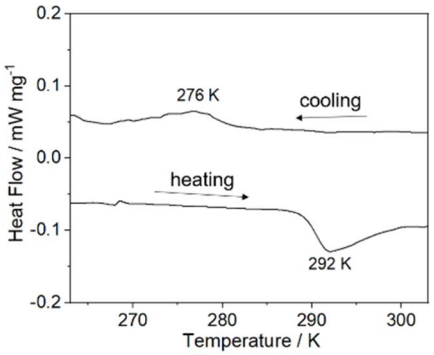

Fig. 2 The DSC curves of **1DySeCN**.

To investigate whether the phase transition affects the local geometry of the Dy^{III} ion and the stacking of the anthracene groups, we determined the single-crystal structure of **1DySeCN** at 193 K and named it **1DySeCN-193**. Interestingly, **1DySeCN-193** crystallizes in a triclinic $P\bar{1}$ space group, which is different from that measured at 293 K (Tables 1 and S1†). The asymmetric unit consists of one Dy^{III} ion, two $SeCN^-$, one NO_3^-, two depma and two 4-hpy ligands (Fig. 1c). Apparently, the phase transition upon cooling is accompanied by a shift from disorder to order in the axial 4-hpy (Fig. S5†). In addition, we also observe slight changes in bond lengths and angles. Compared with those in **1DySeCN-293**, the Dy–O_{ax} bond lengths in **1DySeCN-193** are slightly elongated while the O_{ax}–Dy–O_{ax} angles and Dy–O_{eq} bond lengths are slightly reduced (Tables 1 and S2†). The most significant structural change is probably the stacking of the anthracene units. In **1DySeCN-293**, there is only one type of depma ligand in the structure, and the neighbouring anthracene rings are face-to-face π–π interacted with a d_{cc} distance of 3.759 Å, forming an equally spaced supramolecular chain (Fig. 1b). While in **1DySeCN-193**, there are two types of depma ligands (P1-An, P2-An) in the structure, each of them is face-to-face π–π interacted with its equivalent and the d_{cc} distances are 3.713 Å for P1-An···P1-An and 3.835 Å for P2-An···P2-An, respectively, hence forming an alternatively spaced supramolecular chain (Fig. 1d).

When the measured temperature was further lowered to 130 K, the obtained **1DySeCN-130** crystallizes in the same triclinic $P\bar{1}$ space group, but the cell volume decreases from 2562.4(3) $Å^3$ at 193 K to 2536.1(5) $Å^3$ at 130 K (Tables 1 and S1†). Again, the mononuclear molecules are stacked forming an alternatively arranged supramolecular chain (Fig. 1e and f). Compared to **1DySeCN-193**, the d_{cc} and $d_{C2–C9A}$ spacings of the P1-An···P1-An pair in **1DySeCN-130** increase slightly by 0.011 Å and 0.011 Å, while those of the P2-An···P2-An pair decrease by 0.028 Å and 0.043 Å, respectively (Table 1).

Clearly, lowering temperature leads to a more pronounced differentiation of the two pairs of anthracene rings and a greater deviation of each pair from the face-to-face stacking pattern. The extent to which the anthracene rings deviate from strict face-to-face stacking can be expressed in terms of the slipping angle (θ), *i.e.*, the angle between the centroid–centroid line and the vertical line. The slipping angles of the anthracene rings are 21.91^0 for **1DySeCN-293**, 22.04^0/23.03^0 for **1DySeCN-193**, and 22.44^0/24.49^0 for **1DySeCN-130** (Fig. S6†). Indeed, the slipping angle of the anthracene pairs increases with decreasing temperature. This deviation of anthracene stacking in **1DySeCN** may affect its photophysical properties.

Photophysical properties and photoinduced SC–SC structural transformation of 1DySeCN at room temperature

We first measured the solid-state UV-visible diffuse reflectance spectrum of **1DySeCN** at room temperature. As shown in Fig. 3a, a broad absorption band is observed in the range of 250–450 nm, attributed to the π → π* transition of the depma ligand. In addition, there appears weak absorption peaks at 747 and 756 nm, arising from the f–f transition of the Dy^{III} from $^6H_{15/2}$ to $^6F_{3/2}$.

Fig. 3b shows the PL spectra of the bulk sample of **1DySeCN** as a function of irradiation time, measured on an Edinburgh FLS 980 instrument. The irradiation of the sample at 395 nm (100 mW cm^{-2}) was performed outside the spectrometer prior to PL measurement at 365 nm. Clearly, before UV light irradiation, **1DySeCN** exhibits a broad and strong emission band peaking at 550 nm (λ_{ex} = 365 nm) with an average lifetime (τ) of 25.35 ns, attributed to the excimer emission of the face-to-face stacked anthracene pair (Table S5†). The quantum yield is 6.22%. After exposure to the 395 nm light, the intensity of the excimer emission decreases continuously with increasing irradiation time. At the same time, new peaks appeared at 424, 446, and 575 nm. The average lifetimes of the peaks at 422 and 446 nm are 2.3 and 4.2 ns, respectively, which are much shorter than that of the excimer emission at 550 nm and can be attributed to the π ← π* transition of the dianthracene moiety.[35,36] The shoulder peak at 575 nm correspond to the f–f transition of the Dy^{III} ion from $^4F_{9/2}$ to $^6H_{13/2}$, with phosphorescent lifetime of 7.01 μs (Table S5†). Clearly, photodimerization of the anthracene pairs in **1DySeSCN** occurs after UV illumination, and this enhances the energy of the ^3T state leading to the sensitization of the f–f transition of the dysprosium ion.

Single crystal structural analysis can provide structural information after photoinduced phase transition. By irradiating single crystals of **1DySeCN** under 395 nm UV light (100 mW cm^{-2}) at room temperature for 30 min, we obtained $[Dy^{III}(SeCN)_2(NO_3)(depma_2)(4\text{-hpy})_2]_n$ (**2DySeCN**). Although the

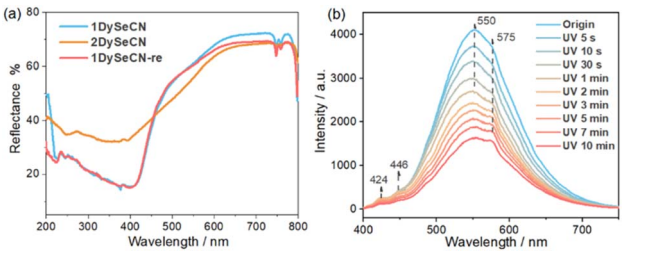

Fig. 3 (a) The solid-state UV-vis spectra of **1DySeCN**, **2DySeCN** and **1DySeCN-re** at room temperature. (b) Photoluminescence spectra of **1DySeCN** as a function of irradiation time upon 395 nm UV-light irradiation (λ_{ex} = 365 nm).

resulting crystals were slightly cracked, they were still suitable for single crystal structure determination. Compound **2DySeCN** measured at 293 K (named as **2DySeCN-293**) crystallizes in the monoclinic system, space group $P2_1/m$. It has a 1D chain structure in which the equivalent Dy^{III} ions are connected by the photo-dimerized $depma_2$ ligands. The central C2–C9A distance in $depma_2$ is 1.658 Å, which is remarkably shortened compared to that in **1DySeCN-293** (3.735 Å). The photodimerization of anthracene pairs also causes changes in the coordination environment of the dysprosium ion (Tables 1 and S2†). The axial Dy–O bond lengths are slightly shortened [2.208(9)/2.231(8) Å *vs.* 2.250(10)/2.222(11) Å in **1DySeCN-293**], and the O7–Dy1–O8 angle becomes slightly smaller [162.4(6)° *vs.* 163.2(4)° in **1DySeCN-293**]. Meanwhile, the equatorial Dy–O/N bond lengths are either elongated or shortened [2.307(7)–2.568(10) Å *vs.* 2.313(6)–2.576(8) Å in **1DySeCN-293**]. The shortest Dy···Dy distance (9.584 Å) is smaller than that in **1DySeCN-293** (9.754 Å). Variations in these structural parameters explain the changes in the PL profiles of **1DySeCN-293** upon UV irradiation. Also, they will lead to changes in the magnetic properties (shown below).

Notably, the SC–SC structural transformation from **1DySeCN** to **2DySeCN** is reversible by annealing **2DySeCN** at 105 °C. The process can be repeated at least five times with retaining the single crystallinity (Table S6 and Fig. S7†). It is worth mentioning that although one axial 4-hpy in **2DySeCN-293** is disordered, we did not see an order–disorder phase transition down to 150 K, as confirmed by the single crystal structural analysis at 193 K (Table S2 and Fig. S8†) as well as the DSC analysis in the temperature range 150–303 K (Fig. S3b†).

To ensure the completeness of the photocycloaddition reaction of the bulk sample for physical measurements, we irradiated the crystals of **1DySeCN** under 395 nm UV light for 12 hours at room temperature. The purity of the resulting **2DySeCN** was confirmed by its PXRD pattern which agrees well with that simulated from the single crystal data (Fig. S1†). In addition, the ^{1}H NMR spectrum of **2DySeCN** digested in DMSO-d_6 solution was also measured. By integrating the area of the two sets of signals (anthracene and dianthracene), we calculated the yield of the photochemical reaction to be 95.2% (Fig. S9–S11†). The DSC curve of **2DySeCN** shows an exothermic peak at 105 °C (ΔH = −51.27 kJ mol^{-1}), indicating the occurrence of de-dimerization of the dianthracene ligand in **2DySeCN** (Fig. S12†). Indeed, by annealing **2DySeCN** at 105 °C for 10 min, it can be transformed back to the pristine **1DySeCN** (named as **1DySeCN-re**). This reversed structural transformation was supported by the PXRD, IR, UV-vis, and PL spectra measurements (Fig. 3a, S1, S13 and S14†).

Effect of temperature on the photophysical and photochemical properties of 1DySeCN

To investigate the temperature effect on the photoluminescent properties of **1DySeCN**, we selected a single crystal and investigated the temperature dependent PL spectra down to 77 K on a Horiba-JY HR Evolution instrument. As shown in Fig. 4a, **1DySeCN** displays a broad and nearly symmetric emission band at 550 nm in the temperature range of 300–180 K, originating

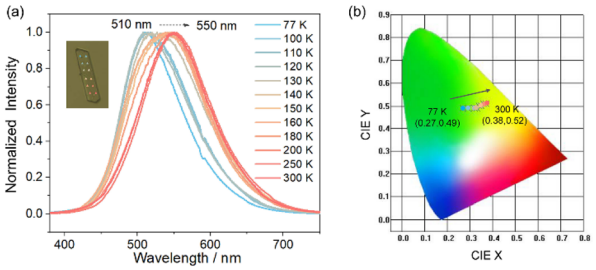

Fig. 4 (a) PL spectra of compound **1DySeCN** with increasing temperature (λ_{ex} = 375 nm), inset: single crystal samples used for measurement and test positions at different temperatures; (b) the CIE graph of **1DySeCN** in the range 77–300 K.

from the excimer emission of the π–π stacked anthracene pairs. The emission band is gradually blue-shifted and becomes more asymmetric at temperatures lower than 160 K. When the temperature is lowered to 100 K, we observe a significant blueshift of the excimer emission from 550 nm to 510 nm. If the temperature is further lowered to 77 K, the position of the excimer emission remains unchanged. At the same time, the luminescence colour changes from bright yellow at 150–300 K to cyan-green at 77–100 K (Fig. 4b), which is a feature of thermochromism. Apparently, this thermochromic property is related to the structural changes of the compound at low temperatures. As mentioned earlier, **1DySeCN-193** and **1DySeCN-130** contain two types of anthracene pairs with slightly different d_{cc} distances and slipping angles, which may account for the blue-shift of the excimer emission (Fig. 1b–f). The fluorescence lifetime of **1DySeCN** at 77 K was 32.17 ns, which is an enhancement of 6.82 ns over that at room temperature (Table S5†), attributed to the weakening of non-radiative processes at low temperatures.[37]

The effect of temperature is more pronounced for the photochemical reaction of **1DySeCN**. In general, lowering the temperature will result in a decrease in the number of molecules in the activated state, thus reducing the rate of reaction. In order to determine the lowest temperature at which the photocycloaddition reaction can occur in a reasonable amount of time, we placed **1DySeCN** crystals on a hot pot and irradiated them *in situ* with 395 nm UV light for 2 h at different temperatures (140–200 K). The resulting samples were subjected to ^{1}H NMR, IR and PXRD measurements (Fig. 5, S15 and S16†). As shown in Fig. 5, we calculated the yields of photochemical reactions of **1DySeCN** in the temperature range of 200–140 K to be 40.8%, 21.6%, 9.5% and 6.8%, respectively. In addition, at temperatures as low as 180 K, the weak vibration peak (686 cm^{-1}) characteristic of the dimerized anthracycline of **1DySeCN** can still be observed after UV illumination (Fig. S15†). Moreover, the PXRD pattern of **1DySeCN** after UV irradiation at 180 K also shows peaks corresponding to **2DySeCN** (Fig. S16†). When the temperature further decreases to 160 and 140 K, these weak characteristic peaks almost disappeared in the IR and PXRD profiles.

To examine the changes in luminescence after UV light irradiation, we selected a single crystal of **1DySeCN** and studied the PL spectra after irradiation for different times at low

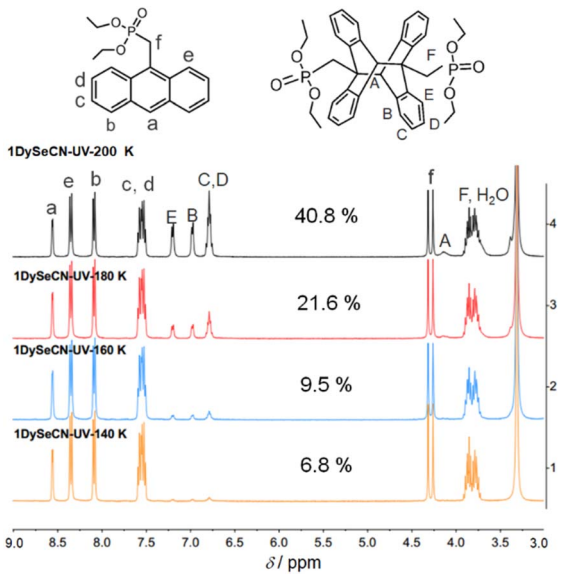

Fig. 5 The ^{1}H NMR spectra in the range of 9.0–3.0 ppm of **1DySeCN** irradiated *in situ* with 395 nm UV light for 2 h at different temperatures (140–200 K) in DMSO-d_6.

temperatures (77–275 K) using a home-built fluorescence microscope. Due to the limited light sources available for this instrument, we used a 375 nm laser for UV irradiation and excitation with power of 9570 W cm^{-2}. As shown in Fig. 6, the PL spectrum of the **1DySeCN** single crystal at 300 K is identical to that of the bulk sample, showing a broad excimer emission peaking at 550 nm. Upon 375 nm light irradiation, photocycloaddition reactions occurred which can be monitored by its PL spectra. The intensity of the excimer emission decreased with increasing irradiation time, while the intensity of the dianthracene emission at 422 and 446 nm increased. In addition, shoulder peaks corresponding to the f–f transition of the Dy^{III} ion appeared at 575 nm. A similar change in the PL profile was observed when the photoreaction temperature was lowered to 200–275 K. Notably, when the temperature was further reduced, the emission intensity of dianthracene and the Dy^{III} ion became very weak at 175 K and invisible below 150 K. The results imply that at temperatures as low as 175–200 K, **1DySeCN** can undergo an efficient photocycloaddition reaction concomitant with significant changes in luminescence.

Similar experiments were conducted for crystals of the dilute sample $[Dy_{0.05}Y_{0.95}(SeCN)_2(NO_3)(depma)_2(4\text{-hpy})_2]$ (**1DySeCN@Y**) at low temperatures (77–300 K). Upon UV light irradiation, we observed a significant reduction of the excimer emission intensity (Fig. S17†). Although the PL spectra did not show distinct characteristic emission peaks of dianthracene, the ^{1}H NMR characterization showed the yields of photochemical reactions of **1DySeCN@Y** to be 33.3% at 200 K, 25.4% at 180 K, 15.7% at 160 K and 8.3% at 140 K, respectively (Fig. S18†). Notably, the yield may be affected by the amount of sample placed on the hot stage and how it is placed.

We also tried to analyse the structure of the resulting crystal (named as **2DySeSCN-200**) after irradiating **1DySeCN** *in situ* with 395 nm UV light for 30 min at 200 K. Unfortunately, the atoms in **2DySeSCN-200** were severely disordered, so we were unable to solve the structure. However, the fact that the atoms are heavily disordered indirectly supports the occurrence of photodimerization of anthracene pairs in **1DySeCN** at 200 K.

Photo-switchable magnetic properties of 1DySeCN

Fig. S19† shows the dc magnetic susceptibilities of **1DySeCN** and **2DySeCN** measured under an applied dc field of 1 kOe in the temperature range of 2–300 K. The $\chi_M T$ values at 300 K are 14.10 and 14.01 cm^3 K mol^{-1} for **1DySeCN** and **2DySeCN**, respectively, consistent with the theoretical value of 14.17 cm^3 K mol^{-1} for an isolated Dy^{III} ($^6H_{15/2}$, $S = 5/2$, $L = 5$, $g_J = 4/3$). In both cases, $\chi_M T$ decreases gradually with decreasing temperature until 5 K, ascribed to the depopulation of Stark sublevels. Below 5 K, the $\chi_M T$ declines sharply, which may be due to the blocking of the magnetic moment.[38] The unsaturated magnetization (M) values at 2 K and 70 kOe (5.19 Nβ for **1DySeCN**, 5.68 Nβ for **2DySeCN**) as well as the non-superposition of the *M vs. H*/*T* plots at different temperatures suggested the presence of magnetic anisotropy and/or low-lying excited states (Fig. S20†). Interestingly, both compounds exhibit butterfly-shaped hysteresis loops (Fig. S21†), but the loop for **2DySeCN** is significantly narrowed compared to that of **1DySeCN** (Fig. S21b†). The closing of the hysteresis loops at zero dc field indicates that strong quantum tunnelling of magnetization (QTM) is operative in both cases,[39] possibly due to the weak magnetic interactions between the dysprosium ions.

To inhibit the QTM effect, we prepared the diluted sample $[Dy_{0.05}Y_{0.95}(SeCN)_2(NO_3)(depma)_2(4\text{-hpy})_2]$ (**1DySeCN@Y**), and its photodimerization product $[Dy_{0.05}Y_{0.95}(SeCN)_2(NO_3)(depma_2)(4\text{-hpy})_2]$ (**2DySeCN@Y**). **1DySeCN@Y** also exhibited reversible photochemical reactions upon UV irradiation, as confirmed by PXRD, IR, UV-vis diffuse reflectance and emission spectra as well as dc magnetic susceptibility measurements (Fig. S22† and 7a). The magnetization values are again not saturated for **1DySeCN@Y** and **2DySeCN@Y** at 2 K and 70 kOe (Fig. S23†). Remarkably, **1DySeCN@Y** shows open butterfly-shaped hysteresis loops below 4 K characteristic of SMM behaviour (Fig. 7b and S24a†), indicating that QTM is effectively suppressed below this temperature (T_B).[40] The remnant and coercivity values at 2 K are 0.56 Nβ and 1200 Oe, respectively. By contrast, **2DySeCN@Y** displays open hysteresis loops below 3 K with smaller remnant (0.24 Nβ) and coercivity (200 Oe) values at 2 K (Fig. 7b and S24b†). The zero-field-cooling (ZFC) and field-cooling (FC) χ_M *vs.* T curves show clear divergences at 4.2 K for **1DySeCN@Y** and 3.4 K for **2DySeCN@Y**, indicating that the blocking temperatures (T_B) are 4.2 K and 3.4 K for the two compounds, respectively (Fig. 7c and d). Notably, the remnant, coercivity and T_B values of **1DySeCN@Y** are all the highest among the known photo-responsive luminescent Ln-SMMs (Table S7†).

To further understand the magnetic dynamics, we performed the alternating current (ac) susceptibility measurements of **1DySeCN** and **2DySeCN** under zero dc field. Both show temperature and frequency dependences of the in-phase (χ') and out-of-phase (χ'') susceptibility components typical for

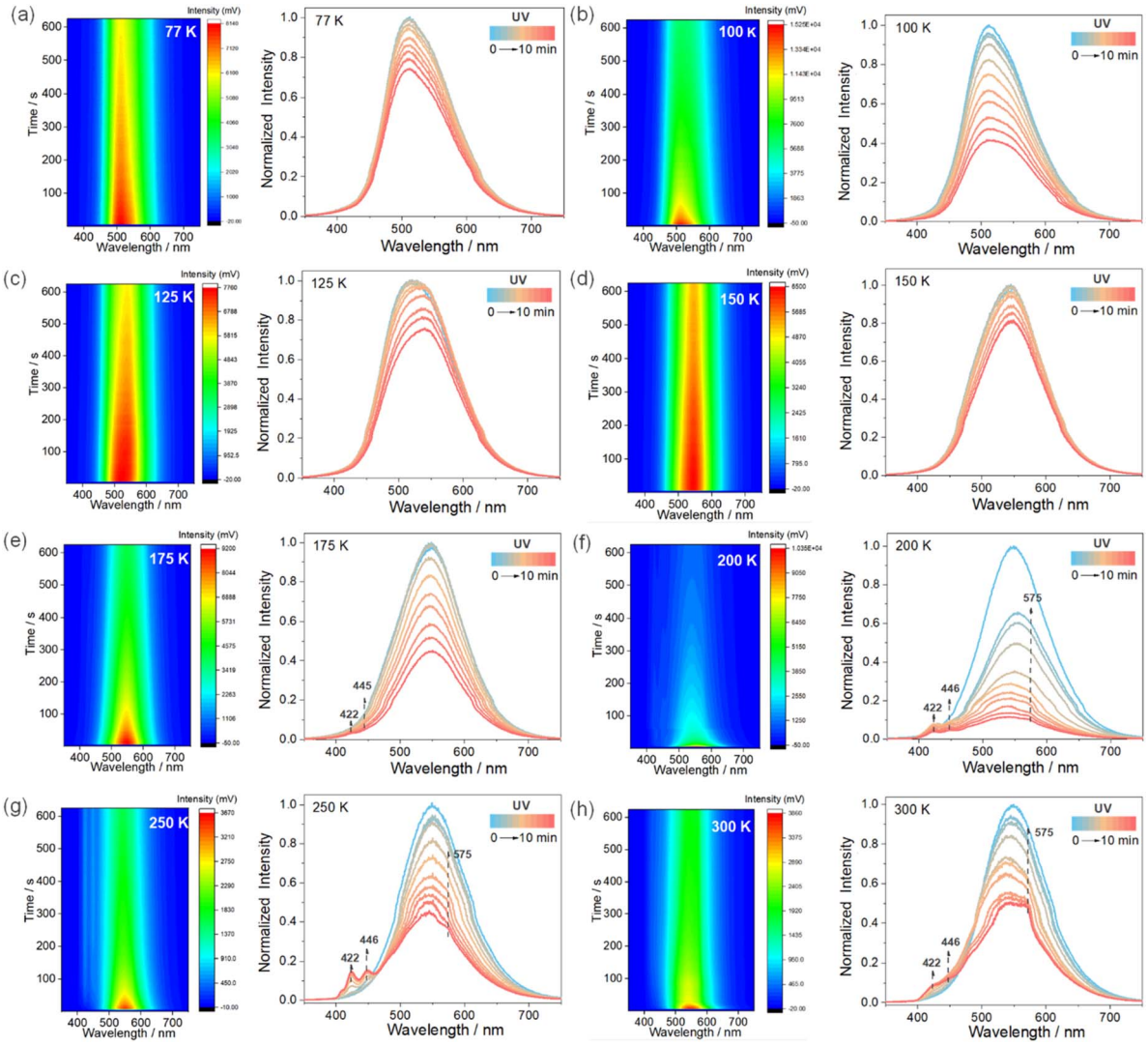

Fig. 6 (a–h) (Left) Real-time photoluminescence spectral change of **1DySeCN** in the range 77–300 K under excitation at 375 nm. (Right) Selected photoluminescence spectra at different times (1 s, 3 s, 5 s, 10 s, 30 s, 1 min, 2 min, 3 min, 5 min, 7 min, 10 min) represent the photodimerization process after UV irradiation.

SMMs (Fig. S25 and S26†). The relaxation times (τ) were extracted using the generalized Debye model,[41] and both exhibit a broad distribution of relaxation coefficients, *e.g.* $\alpha = 0.08$–0.31 (2–22 K) for **1DySeCN** and $\alpha = 0.15$–0.32 (2–14 K) for **2DySeCN** (Tables S8 and S9†). The $\ln \tau$ *vs.* T^{-1} curves can be fitted using eqn (1), which considers the QTM, Raman, and Orbach processes.

$$\tau^{-1} = {\tau_{\mathrm{QTM}}}^{-1} + CT^{n} + {\tau_0}^{-1}\exp\left(\frac{-U_{\mathrm{eff}}}{k_{\mathrm{B}}T}\right) \quad (1)$$

$$\tau^{-1} = CT^{n} + {\tau_0}^{-1}\exp\left(\frac{-U_{\mathrm{eff}}}{k_{\mathrm{B}}T}\right) \quad (2)$$

where U_{eff} is the effective energy barrier of the Orbach process. For **1DySeCN**, the resulting parameters are $U_{\mathrm{eff}} = 334(24)$ K, $\tau_0 = 1.5(2) \times 10^{-11}$ s, $C = 8(5) \times 10^{-4}$ K$^{-4.55}$ s^{-1}, $n = 4.5(3)$, $\tau_{\mathrm{QTM}} = 0.057(2)$ s. While for **2DySeCN**, the parameters are $U_{\mathrm{eff}} = 144(17)$ K, $\tau_0 = 6.2(7) \times 10^{-8}$ s, $C = 0.4(2)$ K$^{-2.54}$ s^{-1}, $n = 2.5(2)$, $\tau_{\mathrm{QTM}} = 0.011(3)$ s. Clearly, the photoinduced structural transformation from **1DySeCN** to **2DySeCN** causes a drastic change in SMM behaviour with the reduction of the effective energy barrier by more than a half and an acceleration of the magnetic relaxation, which can be related to the weakening of the magnetic anisotropy around the Dy^{III} ion after photocycloaddition reaction.

The diluted samples **1DySeCN@Y** and **2DySeCN@Y** also show slow magnetic relaxation at zero dc field (Fig. 7e, f, S27, S28, Tables S10 and S11†). The $\ln \tau$–T^{-1} curves for **1DySeCN@Y** and **2DySeCN@Y** were fitted with eqn (2) containing Orbach and Raman processes. The resulting parameters are $U_{\mathrm{eff}} = 347(11)$ K, $\tau_0 = 5.9(3) \times 10^{-12}$ s, $C = 7(1) \times 10^{-6}$ K$^{-6.23}$ s^{-1}, and $n = 6.2(1)$ for **1DySeCN@Y**, and $U_{\mathrm{eff}} = 207(12)$ K, $\tau_0 = 1.4(3) \times 10^{-9}$ s, $C = 1.2(4) \times 10^{-3}$ K$^{-4.56}$ s^{-1}, and $n = 4.6(2)$ for **2DySeCN@Y**, respectively. Apparently, the energy barrier of the diluted sample is larger than that of the pristine samples, attributed to the suppression of the QTM effect.

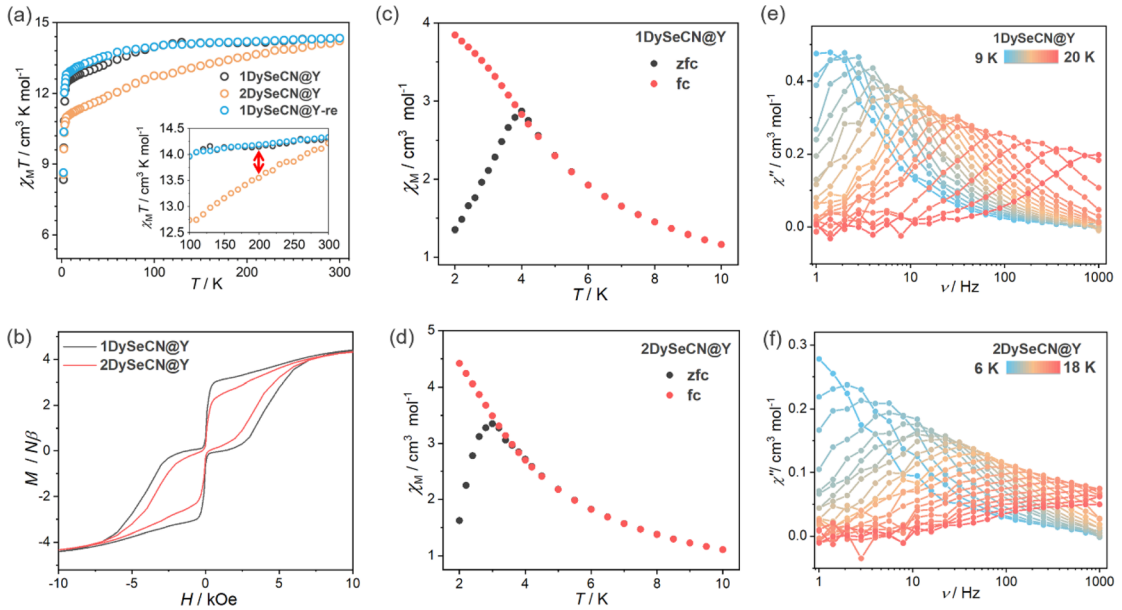

Fig. 7 (a) The temperature-dependent $\chi_M T$ products for compounds **1DySeCN@Y**, **2DySeCN@Y** and **1DySeCN@Y-re**, inset: local enlargement in the temperature range 180–200 K; (b) the magnetic hysteresis curves for **1DySeCN@Y** and **2DySeCN@Y** at 2 K with a sweep rate of 200 Oe s^{-1}; (c and d) The zfc–fc curves for **1DySeCN@Y** and **2DySeCN@Y** with a temperature sweep rate of 0.5 K min^{-1}. (e and f) The frequency dependence of the out-of-phase χ'' of the ac susceptibilities for **1DySeCN@Y** and **2DySeCN@Y**.

The above results demonstrate that the photocycloaddition reaction of **1DySeCN** and its dilute sample **1DySeCN@Y** will cause remarkable changes in their SMM behavior, *i.e.*, the reduction of effective energy barrier and the narrowing of the hysteresis loop. However, the temperature at which the SMM behaviour was observed ($T_B \leq 4.2$ K) differed significantly from the temperature at which the photocycloaddition reaction was observed (≥140 K). An interesting finding is that the $\chi_M T$ values of **1DySeCN@Y** and its photodimerization product **2DySeCN@Y** are quite different at about 175–200 K (Fig. 7a). This result, combined with the fact that **1DySeCN@Y** can undergo photocycloaddition reaction at 175–200 K and produce notable luminescence changes (Fig. S16†), makes it possible to synergistically modulate the magnetic and luminescent properties of Ln-SMMs at the same temperature *via* a reversible *in situ* photocycloaddition reaction. Similar work has not yet been seen in the literature.

Conclusions

We report a dysprosium–anthracene single-molecule magnet, namely $[Dy(SeCN)_2(NO_3)(depma)_2(4\text{-hpy})_2]$ (**1DySeCN**). The significance of this work is three-fold. First, **1DySeCN** and its dilute sample (**1DySeCN@Y**) show the highest effective energy barrier for magnetization reversal and blocking temperature among the known photoresponsive luminescent Ln-SMMs. Second, **1DySeCN** is capable of undergoing photoinduced SC–SC structural transformation accompanied by remarkable changes in luminescence and SMM behaviour. Third, the temperature at which the anthracene groups in **1DySeCN** and **1DySeCN@Y** undergo efficient photodimerization can be as low as 175–200 K, along with notable changes in magnetic and luminescent properties. This work may shed light on the development of photoresponsive luminescent Ln-SMMs for practical applications.

Data availability

Crystallographic data for complexes **1DySeCN** (**1DySeCN-293**, **1DySeCN-193**, **1DySeCN-130**) and **2DySeCN** (**2DySeCN-293**, **2DySeCN-193**) have been deposited at the **https://www.ccdc.cam.ac.uk/structures/** with the deposition numbers CCDC 2421525–2421527, 2424230 and 2424231. The data supporting this article have been included as part of the ESI.†

Author contributions

X.-F. M. conducted most of the experiments and wrote the draft of the manuscript. X.-L. H. and Y.-X. T. performed single crystal PL measurements at low temperature and the related data processing. Y.-H. Q. assisted in the NMR measurements of the photo-dimerized products. Q. T. assisted in performing the single-crystal X-ray diffraction data collection. S.-S. B. assisted in single crystal structural analysis. L.-M. Z. conceived the project and revised the manuscript.

Conflicts of interest

There are no conflicts to declare.

Acknowledgements

This work was supported by grants from the National Natural Science Foundation of China (22273037, 21731003).

Notes and references

1 E. Coronado, Molecular magnetism: from chemical design to spin control in molecules, materials and devices, *Nat. Rev. Mater.*, 2020, **5**, 87–104.
2 J. J. Zakrzewski, M. Liberka, J. Wang, S. Chorazy and S.-i. Ohkoshi, *Chem. Rev.*, 2024, **124**, 5930–6050.
3 N. Deorukhkar, C. Egger, L. Guénée, C. Besnard and C. Piguet, *J. Am. Chem. Soc.*, 2024, **146**, 308–318.
4 P. Sadhukhan, S.-Q. Wu, S. Kanegawa, S.-Q. Su, X. Zhang, T. Nakanishi, J. I. Long, K. Gao, R. Shimada, H. Okajima, A. Sakamoto, J. G. Chiappella, M. S. Huzan, T. Kroll, D. Sokaras, M. L. Baker and O. Sato, *Nat. Commun.*, 2023, **14**, 3394.
5 R. Marin, G. Brunet and M. Murugesu, *Angew. Chem., Int. Ed.*, 2021, **60**, 1728–1746.
6 K. Bernot, C. Daiguebonne, G. Calvez, Y. Suffren and O. Guillou, *Acc. Chem. Res.*, 2021, **54**, 427–440.
7 J. Long, Y. Guari, R. A. S. Ferreira, L. D. Carlos and J. Larionova, *Coord. Chem. Rev.*, 2018, **363**, 57–70.
8 Y.-C. Chen and M.-L. Tong, *Chem. Sci.*, 2022, **13**, 8716–8726.
9 V. Vieru, S. Gómez-Coca, E. Ruiz and L. F. Chibotaru, *Angew. Chem., Int. Ed.*, 2024, **63**, e202303146.
10 K. Dhbaibi, M. Grasser, H. Douib, V. Dorcet, O. Cador, N. Vanthuyne, F. Riobé, O. Maury, S. Guy, A. Bensalah-Ledoux, B. Baguenard, G. L. J. A. Rikken, C. Train, B. Le Guennic, M. Atzori, F. Pointillart and J. Crassous, *Angew. Chem., Int. Ed.*, 2023, **62**, e202215558.
11 H. Huang, R. Sun, X.-F. Wu, Y. Liu, J.-Z. Zhan, B.-W. Wang and S. Gao, *Dalton Trans.*, 2023, **52**, 7646–7651.
12 O. Cador, B. Le Guennic and F. Pointillart, *Inorg. Chem. Front.*, 2019, **6**, 3398–3417.
13 Z. Zhu, X.-L. Li, S. Liu and J. Tang, *Inorg. Chem. Front.*, 2020, **7**, 3315–3326.
14 X. Gou, Y. Wu, M. Wang, N. Liu, W. Lan, Y.-Q. Zhang, W. Shi and P. Cheng, *Dalton Trans.*, 2024, **53**, 148–152.
15 J. Li, M. Kong, L. Yin, J. Zhang, F. Yu, Z.-W. Ouyang, Z. Wang, Y.-Q. Zhang and Y. Song, *Inorg. Chem.*, 2019, **58**, 14440–14448.
16 R. Jankowski, M. Wyczesany and S. Chorazy, *Chem. Commun.*, 2023, **59**, 5961–5986.
17 L. Münzfeld, M. Dahlen, A. Hauser, N. Mahieu, S. K. Kuppusamy, J. Moutet, M. Tricoire, R. Köppe, L. La Droitte, O. Cador, B. Le Guennic, G. Nocton, E. Moreno-Pineda, M. Ruben and P. W. Roesky, *Angew. Chem., Int. Ed.*, 2023, **62**, e202218107.
18 N. Monni, J. J. Baldoví, V. García-López, M. Oggianu, E. Cadoni, F. Quochi, M. Clemente-León, M. L. Mercuri and E. Coronado, *Chem. Sci.*, 2022, **13**, 7419–7428.
19 M.-J. Liu, Z.-Y. Fu, R. Sun, J. Yuan, C.-M. Liu, B. Zou, B.-W. Wang and H.-Z. Kou, *ACS Appl. Electron. Mater.*, 2021, **3**, 1368–1374.
20 (*a*) M. Hojorat, H. Al Sabea, L. Norel, K. Bernot, T. Roisnel, F. Gendron, B. L. Guennic, E. Trzop, E. Collet, J. R. Long and S. Rigaut, *J. Am. Chem. Soc.*, 2020, **142**, 931–936; (*b*) K. Rogacz, M. Magott, S. Baś, M. Foltyn, M. Rams and D. Pinkowicz, *RSC Adv.*, 2024, **14**, 14515–14522.
21 Y.-J. Ma, J.-X. Hu, S.-D. Han, J. Pan, J.-H. Li and G.-M. Wang, *J. Am. Chem. Soc.*, 2020, **142**, 2682–2689.
22 H. Kong, J.-Y. Wang, J.-C. Liu, L. Zhang, P.-Y. Liao, Y.-Q. Qi, Z. Liu, S.-G. Wu and M.-L. Tong, *Angew. Chem., Int. Ed.*, 2025, **64**, e202422557.
23 Q. Zhang, S.-D. Han, Q. Li, J.-X. Hu and G.-M. Wang, *Sci. China Mater.*, 2022, **65**, 788–794.
24 P.-Y. Liao, Y. Liu, Z.-Y. Ruan, H.-L. Wang, C.-G. Shi, W. Deng, S.-G. Wu, J.-H. Jia and M.-L. Tong, *Inorg. Chem.*, 2023, **62**, 1075–1085.
25 L. Wu, X.-D. Huang, W. Li, X. Cao, W.-H. Fang, L.-M. Zheng, M. Dolg and X. Chen, *JACS Au*, 2024, **4**, 3606–3618.
26 X.-D. Huang, Y. Xu, K. Fan, S.-S. Bao, M. Kurmoo and L.-M. Zheng, *Angew. Chem., Int. Ed.*, 2018, **57**, 8577–8581.
27 X.-F. Ma, P.-F. Mi, S.-S. Bao and L.-M. Zheng, *Chin. J. Inorg. Chem.*, 2024, **40**, 270–280.
28 X.-D. Huang, G.-H. Wen, S.-S. Bao, J.-G. Jia and L.-M. Zheng, *Chem. Sci.*, 2021, **12**, 929–937.
29 X.-D. Huang, X.-F. Ma, T. Shang, Y.-Q. Zhang and L.-M. Zheng, *Inorg. Chem.*, 2023, **62**, 1864–1874.
30 X.-F. Ma, X.-D. Huang and L.-M. Zheng, *Cryst. Growth Des.*, 2023, **23**, 1095–1103.
31 X.-D. Huang, X.-F. Ma and L.-M. Zheng, *Angew. Chem., Int. Ed.*, 2023, **62**, e202300088.
32 D. Casanova, M. Llunell, P. Alemany and S. Alvarez, *Chem.–Eur. J.*, 2005, **11**, 1479–1494.
33 G. M. J. Schmidt, *Pure Appl. Chem.*, 1971, **27**, 647–678.
34 D.-S. Sun, Y.-Z. Zhang, J.-X. Gao, X.-N. Hua, X.-G. Chen, G.-Q. Mei and W.-Q. Liao, *CrystEngComm*, 2019, **21**, 2669–2674.
35 X.-D. Huang, J.-G. Jia, M. Kurmoo, S.-S. Bao and L.-M. Zheng, *Dalton Trans.*, 2019, **48**, 13769–13779.
36 X.-F. Ma, X.-D. Huang, G.-H. Wen, S.-S. Bao, Y.-Q. Zhang and L.-M. Zheng, *Dalton Trans.*, 2022, **51**, 12026–12030.
37 D.-S. Sun, Y.-Z. Zhang, J.-X. Gao, X.-N. Hua, X.-G. Chen, G.-Q. Mei and W.-Q. Liao, *CrystEngComm*, 2019, **21**, 2669–2674.
38 Y.-S. Meng, L. Xu, J. Xiong, Q. Yuan, T. Liu, B.-W. Wang and S. Gao, *Angew. Chem., Int. Ed.*, 2018, **57**, 4673–4676.
39 J. Wang, Q.-W. Li, S.-G. Wu, Y.-C. Chen, R.-C. Wan, G.-Z. Huang, Y. Liu, J.-L. Liu, D. Reta, M. J. Giansiracusa, Z.-X. Wang, N. F. Chilton and M.-L. Tong, *Angew. Chem., Int. Ed.*, 2021, **60**, 5299–5306.
40 F. Habib, P.-H. Lin, J. Long, I. Korobkov, W. Wernsdorfer and M. Murugesu, *J. Am. Chem. Soc.*, 2011, **133**, 8830–8833.
41 K. S. Cole and R. H. Cole, *J. Chem. Phys.*, 1941, **9**, 341–351.